Chapter 3

The stratigraphic expression of a large negative carbon isotope excursion from the Ediacaran Johnnie Formation, Death Valley

Kristin D. Bergmann[1], Rebecca A. Zentmyer[1], Woodward W. Fischer[1]

[1]California Institute of Technology

originally published in Precambrian Research *v. 188 p. 45-56 © 2011 Elsevier, Inc.*

3.1 Abstract

The Rainstorm Member of the Ediacaran Johnnie Formation of the southern Basin and Range, US, records a large negative excursion in carbon isotope ratios of carbonate strata ($\delta^{13}C_{VPDB} > -6‰$). The character of the excursion raises fundamental questions about whether this isotopic pattern is accurately capturing the time-series behavior of marine dissolved inorganic carbon (DIC) or is a product of diagenesis. To explore this issue, we examined the expression of this isotopic excursion within the Johnnie oolite, a $\sim$ 2 m thick marker bed, which records the highest rate of change in $\delta^{13}C$. Sedimentologically, the oolite unit is thought to be

time transgressive, if the isotopic excursion reflects time-series behavior of the carbon cycle, its expression in the oolite across the basin should systematically align the sections according to their slight diachroneity. Detailed carbon and oxygen isotopic stratigraphy of the oolite at seven different locations indicates the magnitude of the excursion at the base of the oolite is spatially variable such that after a palinspastic reconstruction the sections align along a systematic north-to-south gradient in the isotopic data. The oolite preserved in the Old Dad Mountains, the most southerly section measured, is an outlier to this trend (and the most difficult to ordinate accurately in the reconstruction), showing the largest isotopic range between the onset of carbonate deposition and top of the oolite. Several hypotheses are congruent with these data, but the sum of observations is best explained by a scenario wherein the oolite is time transgressive and deposited in a north-to-south manner throughout the onset of the isotopic excursion. If correct, this implies that the stratigraphic δ^{13}C pattern reflects time-series behavior of marine DIC.

3.2 Introduction

Carbonate-bearing sedimentary successions of Neoproterozoic age record extreme negative excursions in δ^{13}C (and sometimes δ^{18}O) that are distinct from Phanerozoic excursions and difficult to explain because of their unusual geological and geochemical attributes [1, 2, 3, 4]. The most spectacular of these events is known as the Shuram Excursion (SE) because of its discovery in the Shuram Formation of the Nafun Group, Sultanate of Oman [5, 6, 7]. This chemostratigraphic pattern is found in at least four depositional basins separated at the time of deposition (Oman, [5, 2], South Australia, [1], South China, [3, 8], Western USA, [9, 10, 11], but possibly many more (Siberia, [12, **?**], Namibia, [13, 14], Scandinavia, [4, 15], Scotland, [16]). As yet, these excursions lack direct geochronological constraints, but they invite global correlation because they sit, broadly, in middle Ediacaran age strata, between the ∼630 Ma Marinoan glaciation [17] and the Precambrian-

Cambrian boundary at 542 Ma [18, 19]. The excursions are all characterized by $\delta^{13}C_{VPDB}$ values in carbonate-bearing minerals below -6‰. Such light values are considered extreme for a primary marine signal because they exist outside the solution space for carbon isotope mass balance models wherein the isotopic composition of the inputs are often set to presumed mantle values (e.g. [20]). These rocks do not show a corresponding excursion in $\delta^{13}C_{org}$ and tend to be organic lean [1, 2, 8, 21]. Many chemostratigraphic sections also show co-varying $\delta^{13}C$ and $\delta^{18}O$ across both dolomite and calcite lithologies [5, 1, 22, 23]. There is some evidence that these excursions coincide with a drop to more negative $\delta^{34}S_{CAS}$ values [2, 10, 8]. Successions recording the excursions are commonly composed of mixed carbonate and siliciclastic sediments. Purple siltstones and pink carbonates (including calcitic pink ooid grainstone) exist in multiple sections globally, and have a distinctive sequence stratigraphic and lithologic similarity [1, 10, 24, 7, 12]. While robust geochronologic constraints do not exist on the duration and timing of these excursions, they generally span hundreds of meters of stratigraphic thickness [1, 5, 2, 4, 12]. Estimates of the length of time represented by the stratigraphy are on the order of 5-50 million years, far greater than the presumed residence time of carbon in Ediacaran seawater [2, 3, 25, 6], but see [21].

Special interest exists in understanding the nature of these isotopic excursions because of possible connections to a state change in the reduction-oxidation potential of the fluid Earth [26, 2] and timing with regard to the evolution of early animals and algae [27, 2, 28, 8, 29]. Hypotheses that explain a large, long-lived negative excursion in marine dissolved inorganic carbon (DIC) and produce no excursion in coevally deposited organic carbon invoke dynamic models of the carbon cycle wherein the carbon budget includes the demise (via remineralization) of large masses (or proportions) of organic carbon, putatively in the form of dissolved organic carbon (DOC) in seawater [2, 10, 8, 21]. These hypotheses have been criticized from perceived incompatibilities with oxidant chemistry required to remineralize such a large DOC pool [30].

In addition to this criticism, several details of the chemostratigraphic pattern

have raised questions about whether or not this pattern accurately reflects a time-series history of marine DIC. Because carbonate-bearing minerals are often subject to recrystallization and re-equilibration with pore fluids after deposition, the co-varying relationship between $\delta^{13}C$ and $\delta^{18}O$, and the lack of a similar excursion in organic phases has fueled hypotheses that the isotopic excursions have a root diagenetic cause [30, 1, 23, 7, 31]. There are currently two hypotheses that explain the negative excursions using different diagenetic processes. Knauth and Kennedy [23] argued that the excursions are a result of re-equilibration of the rocks with meteoric fluids (low in $\delta^{18}O$) charged with ^{13}C-depleted carbon derived from a somewhat enigmatic terrestrial biosphere. Under their hypothesis, the uniqueness of the chemostratigraphic pattern with regard to timing in Earth history is explained by the proximal evolution of a Neoproterozoic 'phytomass'. Another model suggests that the negative excursions arise from diagenetic processes associated with deep burial diagenesis and re-equilibration at high temperature with fluids charged with isotopically light CO_2 derived from basinal oxidation of hydrocarbons [22]. Under Derry's [22] hypothesis the uniqueness is explained by unusually high organic carbon burial in marine sedimentary basins during Neoproterozoic time (e.g. [32]).

If these excursions are primary signals, it is likely that the carbon isotope systematics during the Neoproterozoic were different than anything revealed in the rock record in the past 500 million years. Many researchers have used these large isotopic excursions as a signal feature to assemble a relative chronology and correlate between sections deposited on different cratons during an interval in Earth's history with few independent chronologic markers [32, 33, 10, 25, 6, 34]. If the excursions resulted from diagenetic processes, then correlating between sections and connecting the signal to a step-wise change in atmospheric oxygen and the evolution of animals and algae would be incorrect. As of yet, a mechanism has not been posited that encompasses all of the observations of this excursion. In this paper, we present the results of a study to further define the stratigraphic and sedimentary context of one such Ediacaran large negative carbon isotope excursion.

A large negative carbon excursion, putatively correlated with the Shuram ex-

cursion [10, 35, 11], is preserved in the Neoproterozoic-aged Johnnie Formation from the Death Valley region, USA [9, 10, 35, 11]. The Johnnie Formation is composed of mixed carbonate and siliciclastic lithologies [36, 37]. The negative excursion is first observed within the Johnnie oolite, a regionally extensive stratigraphic marker composed of a $\sim$ 2 meter thick dolomitic oolite, bounded by 5-40 meter thick purple siltstones. The isotopic rate of change with respect to stratigraphic thickness is rapid in the oolite with documented $\delta^{13}C_{VPDB}$ values ranging from -3.7‰ to -7.3‰ in two meters of stratigraphic section [9, 10, 35, 11]. The $\delta^{13}C_{VPDB}$ values of the limestones overlying the purple siltstones and oolite reach values as low as -12‰ (Fig. 3.1) [10, 35, 11]. The base of the oolite has been interpreted as a time-transgressive surface (e.g., onlapping ooid sand sheet) formed during a regression or transgression because of the dramatic juxtaposition of a shallow-water, high-energy facies on low-energy siltstones and shales [37]. The large range in $\delta^{13}C$, regional extent and sedimentologic character of the oolite provide a useful stratigraphic datum to examine the nature of the excursion in this sedimentary basin. Similar studies have shown the utility of connecting carbon isotope ratios with sequence stratigraphy [38, 39].

We sought to test if the negative $\delta^{13}C$ excursion recorded in the oolite demonstrates a slight diachroneity between seven locations in the southern Basin and Range province due to time-transgressive deposition (Fig. 3.2). If the isotopic composition of the oolite shows clear and systematic basin-scale stratigraphic trends once palinspastically reconstructed, the most parsimonious explanation is that the isotopic signal was a feature present during the formation and deposition of the oolite and thus accurately reflects a negative excursion in marine DIC. No systematic variability across the basin would suggest either synchronous deposition or wholesale diagenetic alteration of any primary signal. Alternatively, clear isotopic variation that is predicted by independent observations of the preservation of petrographic textures would imply that diagenetic processes were responsible for the carbon isotope pattern that defines the excursion.

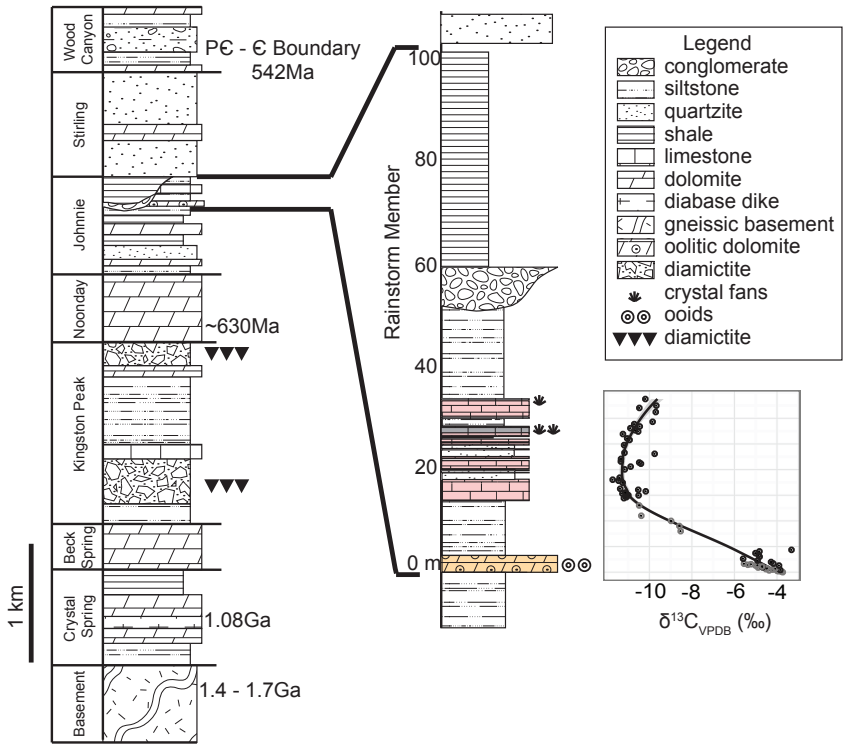

Figure 3.1: Generalized stratigraphy of the Proterozoic strata preserved in the Death Valley region. Center: composite stratigraphic section of the Rainstorm Member of the Johnnie Formation preserved in the southern Nopah Range. Right: carbon isotopic data from the southern Nopah Range location (black) and Johnson Canyon in the Panamint Mountains (grey). The line shown is a moving average, shown with a 95 confidence interval (in grey)

Modified from: [40, 36, 37] and this study

3.3 Geologic setting

The preserved Neoproterozoic stratigraphy in the Death Valley region in the southwestern United States (Fig. 3.1) overlies gneissic (1.7 Ga) and granitic (1.4 Ga) basement [42], and begins with the Pahrump Group, which includes the Crystal Spring Formation, the Beck Spring Formation and Kingston Peak Formation [36]. The Neoproterozoic record also includes the Noonday Formation, Johnnie Formation, Stirling Formation and the lower Wood Canyon Formation (Fig. 3.1) [36]. Robust geochronologic constraints on Pahrump Group strata are rare, diabase dikes within the Crystal Spring Formation yield U/Pb ages of 1087 ± 3 Ma and 1069 ± 3 Ma [43]. The Kingston Peak Formation includes several diamictite hori-

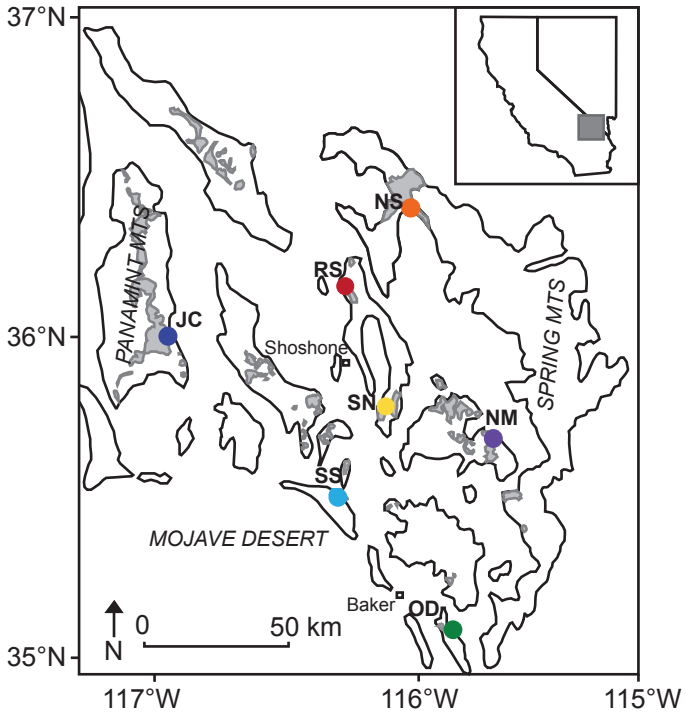

Figure 3.2: Location map of the Death Valley region showing the major mountain ranges and the areal extent of preserved Johnnie Formation in grey. The seven locations examined in this study are marked by colored circles, northern Spring Mountains in orange (NS), Resting Spring Range in red (RS), southern Nopah Range in yellow (SN), Johnson Canyon in the Panamint Mountains in dark blue (JC), northern Mesquite Mountains in purple (NM), Salt Spring Hills in light blue (SS) and the Old Dad Mountains in green (OD).

Modified from: [41, 36]

zons that have been correlated with Neoproterozoic glacial deposits constrained elsewhere to between 723 Ma and 580 Ma [9, 44, 40]. The Noonday Formation, predominately dolomite in composition, includes, at its base, unusual sedimentary features characteristic of Marinoan cap carbonates. It has been correlated to other Marinoan sections using litho- and chemostratigraphy [45, 9, 46], if these correlations are correct, the Noonday is ca. 630 Ma in age. An upper age constraint on the Johnnie Formation comes from paleontological observations. Ediacaran fossils have been documented in the Stirling Formation, and the lowermost Wood Canyon Formation includes the Precambrian-Cambrian boundary, with an implied age of ca. 542 Ma [18, 17, 47, 19, 48, 49]. Within these constraints, the Johnnie Formation was deposited between 630 Ma and 542 Ma, and probably sits in the middle

Ediacaran, deposited between 580 and 550 Ma [10, 50].

This Neoproterozoic through early Cambrian sedimentary sequence records a transition from continental rifting associated with the breakup of Rodinia to the development of a passive margin on western Laurentia [51, 52, 53]. The timing of active rifting is still debated but strong differences in stratigraphic thickness exist in both the Kingston Peak Formation and Johnnie Formation suggesting brief periods of rifting and unequal subsidence, although the possibility remains that the observed incision of the upper Johnnie Formation was glacially driven or part of a marine canyon system [41, 54, 55, 53, 56].

3.3.1 Stratigraphy of the Rainstorm Member

The Johnnie Formation is a mixed siliciclastic and carbonate succession composed of shales, siltstones, quartzites, conglomerates, limestones and dolostones [36], and has been divided into seven sequences [37]. The Johnnie Formation disconformably overlies the Noonday in most locations but extends beyond the outcrop extent of the Noonday and overlies the Kingston Peak Formation in the Silurian Hills and Precambrian basement rocks in the Old Dad Mountains [37]. The Rainstorm Member, the focus of this study, comprising the uppermost Johnnie Formation, includes the siltstones of sequence 5, all of sequence 6 and part of sequence 7 (Fig. 3.1) [37]. This study's reference section of the Rainstorm Member is located in the southern Nopah Range and consists of purple siltstones above and below a $\sim$ 2 meter-thick, ochre-colored, dolomitic oolite. This oolite is colloquially known as the 'Johnnie oolite' because it is an important regional stratigraphic marker (Fig. 3.1 and Fig. 3.3) [36, 37]. Overlying the oolite, the Rainstorm Member continues with orange dolomitic sandstones and pink limestones that include ooid and intraclast grainstones [37]. In the southern Nopah Range, these beds are capped by grey limestone beds containing aragonite crystal fan pseudomorphs (now calcite), which are overlain by more siltstones (Fig. 3.3 and Fig. 3.4) [50, 37]. In several locations, and observable along strike, conglomeratic beds associated with an erosive surface originating from high in the Rainstorm Member incise

deeply into the underlying strata, and can locally contain blocks ∼15 meters in size [54]. This conglomerate unit, thought to be associated with continental rifting or glaciation, is overlain by more siltstones before the boundary with the Stirling Formation (Fig. 3.1) [41, 54, 37].

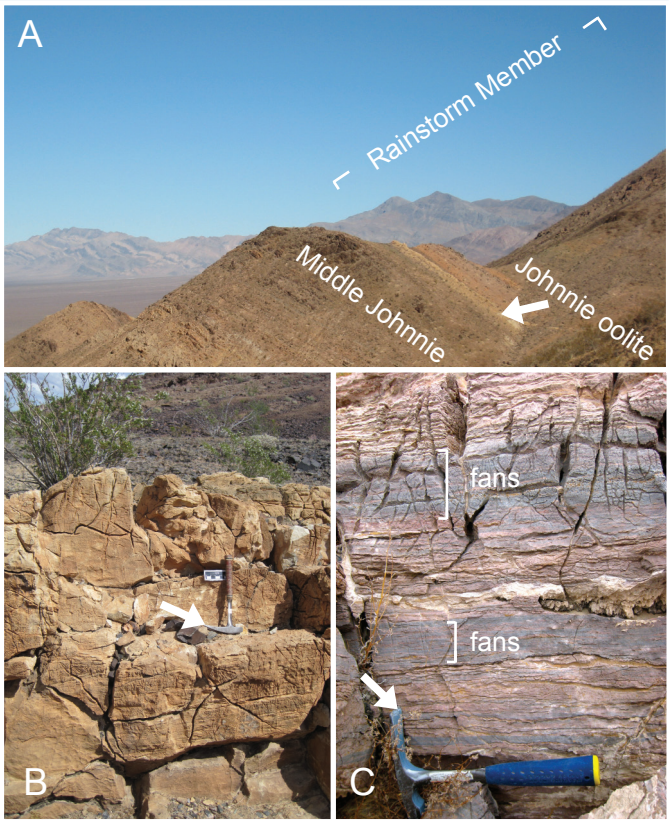

Figure 3.3: a) View of the Rainstorm Member of the Johnnie Formation along a ridge near the Gunsight Mine, southern Nopah Range. The ochre-colored Johnnie oolite marker bed is evident, as are the overlying pink limestone beds. b) Representative photograph of the Johnnie Oolite at the Salt Spring Hills location, note the abundant fractures common to many sections. c) Pink and grey limestone beds in the southern Nopah Range. The pink beds are composed of intraclast grainstone and the grey beds contain aragonite crystal fan pseudomorphs. Rock hammers for scale.

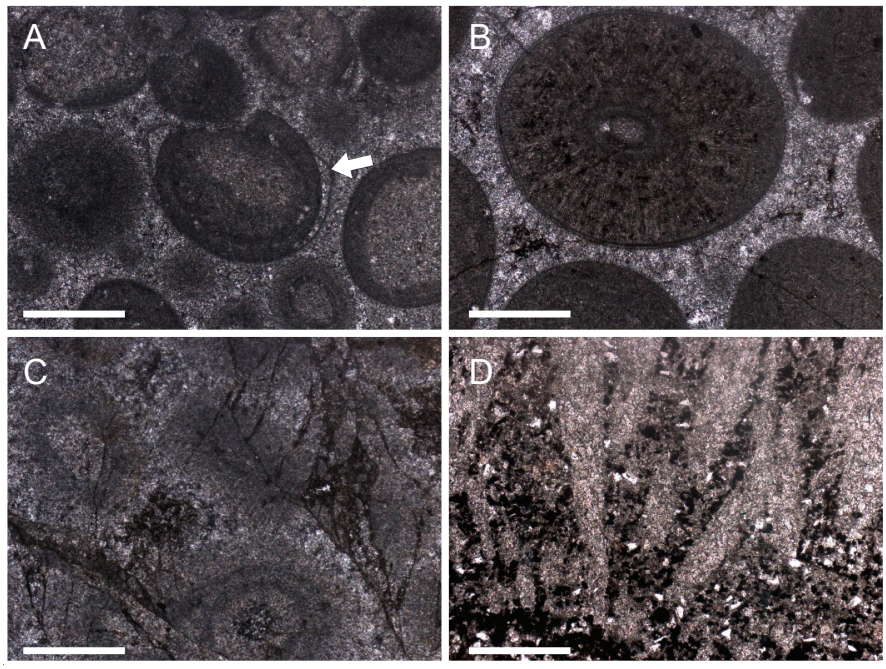

Figure 3.4: Petrography reveals well-preserved textures in many of the Rainstorm Member carbonates. a) Photomicrograph of the Johnnie oolite from the northern Mesquite Mountains. Note the separated ooid cortex. b) Well-preserved radial ooid from the northern Spring Mountains. c) highly fractured oolite from the northern Spring Mountains. Note the poorer preservation of fabrics. d) Aragonite crystal fan pseudomorphs (now calcite) from the grey limestone beds highlighted by hematite and quartz grains from the southern Nopah Range. Scale bar in all photomicrographs is 300 microns.

3.4 Methods

3.4.1 Field work and sample preparation

To examine the sequence stratigraphic nature of the excursion captured by the Rainstorm Member Johnnie oolite, multiple sections were measured and sampled in seven locations across the Death Valley region mountain ranges during the fall of 2008 and the spring and summer of 2010 (Fig. 3.2)(GPS coordinates in Table 3.1). These locations were selected to examine spatial patterns across the preserved sedimentary basin. They also record a large range of post-depositional diagenetic and structural modifications. The Panamint Mountains, for example, were buried deeper and reached much higher peak temperatures compared to the other ranges used in this study [42, 57, 58]. It was evident in the field that some sections show

abundant outcrop-scale faulting of the oolite, these include the Resting Spring Range and the southern Nopah Range [59]. This range of preservation between different locations allows for some testing of diagenetic hypotheses.

The oolite was sampled at very high stratigraphic resolution with samples taken every 10 cm or less. To test the extent of local variability within the carbon and oxygen isotopic systems, two separate oolite sections were sampled $\sim$ 50 m apart at each location. Carbonate beds found above the oolite and below the Johnnie/Stirling Quartzite contact were also sampled and described where present. Hand samples were sectioned with a rock saw to provide unweathered surfaces. Powders for δ^{13}C and δ^{18}O analyses were sampled using a micro-rotary drill with a 2 mm bit targeting regions with well-preserved ooids. Matrix cements were included in the samples but effort was made to avoid fractures and secondary veining. Representative thin sections were made from each section to observe patterns of diagenesis and compare the preservation of carbonate textures between the different locations (Fig. 3.4).

3.4.2 Mass spectrometry

Carbon and oxygen measurements were made at the University of Michigan Stable Isotope Laboratory. Each sample powder was heated to 200°C to remove volatile contaminants and water. 20-30 μg of sample was reacted with anhydrous H_3PO_4 acid at 77° $\pm$ 1°C degrees for 12 minutes. The reaction occurred in a ThermoFinnigan MAT Kiel IV preparation device that directly introduced the evolved CO_2 sample into a ThermoFinnigan MAT 253 gas source mass spectrometer. Isotopic measurements were calibrated against NBS 18 and NBS 19. Accuracy and precision, measured by multiple analyses of known standards, are better than $\pm$ 0.1‰. Isotope ratios for both carbon and oxygen are reported by reference to Vienna Pee Dee Belemnite (VPDB).

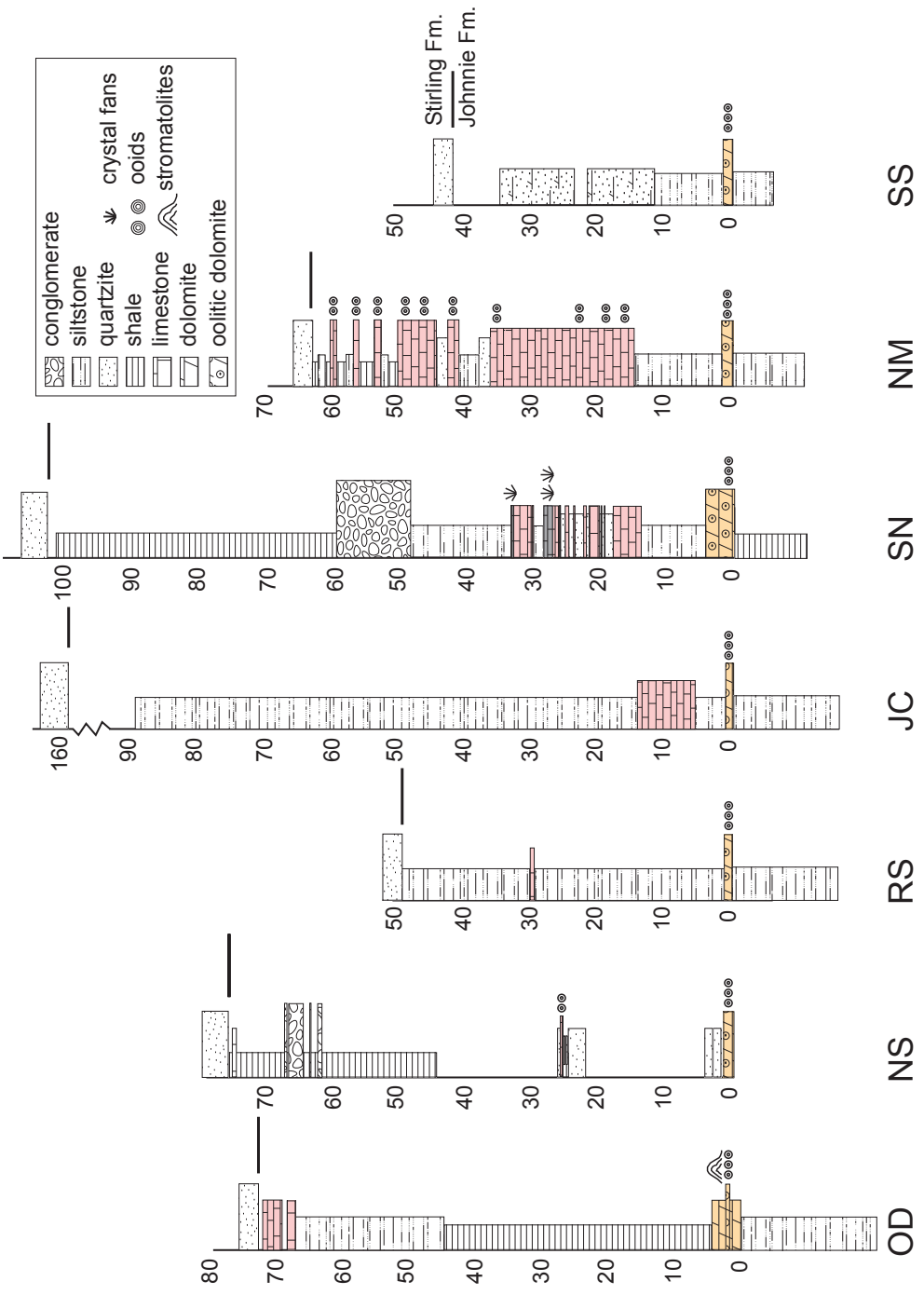

Figure 3.5: Stratigraphic columns of the study locations. The Johnnie oolite (orange) is used as a stratigraphic datum to align the sections. The overlying limestone beds are also highlighted (pink).

Data from this study and [37, 35, 11]

3.5 Results

3.5.1 Northern Spring Mountains (NS)

The northern Spring Mountains section is the northernmost section sampled in this study. The Noonday Formation-Johnnie Formation contact is not exposed but the documented thickness of the Johnnie Formation at this locale is 354 meters [37]. The thickness from the oolite to the contact with the Stirling Formation is $\sim$ 80 meters (Fig. 3.5) [37]. Much of the section above the oolite is covered, but the 1.5 m oolite is well exposed. A thin ($\sim$ 20 cm) pink ooid grainstone bed is located $\sim$ 27 meters above the oolite. Conglomerate beds also appear $\sim$10 meters below the base of the Stirling at this location (Fig. 3.5) [37]. Two sections of the oolite were sampled approximately 50 meters apart. Both sections record declining $\delta^{13}C_{VPDB}$, from -2.9‰ and -3.2‰ at the base to -4.9‰ and -4.9‰ at the top of the oolite (Fig. 3.6). There is good agreement in both the pattern of decline and absolute magnitude of the two sections (Fig. 3.6). In the northern Spring Mountains, the Johnnie oolite is highly fractured compared to other sections and the ooids were not as well preserved in all samples. Nonetheless the $\delta^{13}C$ values show small first differences and a steady decline with stratigraphic height (Fig. 3.4b, c and Fig. 3.6).

3.5.2 Resting Spring Range (RS)

The Johnnie Formation is also incomplete in the Resting Spring Range and the thickness of the Rainstorm Member is variable. In the section measured for this study, the thickness from the oolite to the contact with the Stirling Formation is $\sim$ 50 meters (Fig. 3.5). In the measured section, the oolite is encountered twice, likely due to duplication by a thrust fault. The upper oolite may also be structurally thickened (4 meters versus $\sim$1.3 meters) and the decline in $\delta^{13}C$ occurs over a slightly smaller range (Fig. 3.6). In the two sections sampled from the lower exposure of oolite, $\delta^{13}C_{VPDB}$ values begin at -2.9‰and -2.9‰ and drop to values of -5.3‰ and -4.3‰ over 1.3 meters. $\delta^{13}C$ begins at -4.7‰ in the second oolite and more gradually drops to -5.9‰ at the top (Fig. 3.6). The Resting Spring

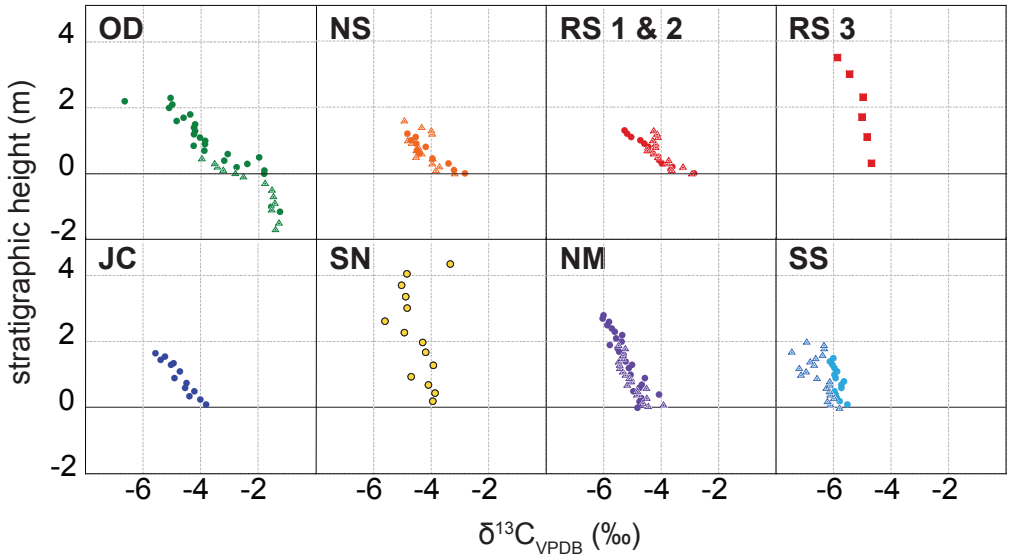

Figure 3.6: $\delta^{13}C_{VPDB}$ data from the measured sections, grouped by location. Multiple sections are distinguished using a solid square and open triangle. The 0 m datum is the base of the oolite at each location. Old Dad Mountains (OD) is shown in green, northern Spring Mountains (NS) in orange, Resting Spring Range (RS) in red, Johnson Canyon (JC) in dark blue, southern Nopah Range (SN) is in yellow, northern Mesquite Mountains (NM) in purple, and Salt Spring Hills (SS) in light blue. The Resting Spring Range has three measured sections because the Johnnie oolite is structurally repeated in the section measured (RS 1, 2 and RS 3).

section also has a very thin (10 cm) bed of pink micritic limestone near the base of the Stirling contact ($\sim$ 30 meters above the upper exposure of oolite). This bed records a $\delta^{13}C_{VPDB}$ value of -8.0‰ (Fig. 3.5). In the Resting Spring Range, the Rainstorm Member is very similar in both lithology and thickness to the northern Spring Mountain section.

3.5.3 Johnson Canyon, Panamint Mountains (JC)

The Johnson Canyon section is located in the Panamint Mountains in Death Valley but is very similar lithologically to Rainstorm Member exposures in the southern Nopah Range. The thickness from the oolite to the contact with the Stirling Formation is $\sim$ 160 meters and is the thickest of this study [35, 11]. The base of the oolite has $\delta^{13}C_{VPDB}$ values of -3.8‰, which decline to -5.6‰ at the top of the oolite. The pink limestones are thicker in Johnson Canyon than in the Spring Mountains and Resting Spring Range and they sit closer to the oolite.

Overlying the oolite are 5 meters of siltstones and 6.5 meters of pink carbonates showing declining $\delta^{13}C_{VPDB}$ values ranging from -8.6‰ to -10.7‰. Rare carbonate beds in $\sim$ 150 meters of siltstone and sandstone below the Stirling contact are also isotopically depleted but become less depleted up section from -11.4‰ to -8.2‰ [35].

3.5.4 Southern Nopah Range (SN)

The Johnnie Formation is well exposed throughout the southern Nopah Range. In the section measured for this study, the thickness from the oolite to the Stirling contact is $\sim$ 100 meters and includes coarse conglomeratic beds. There is evidence that the oolite sampled and measured for this study was structurally thickened from post-deposition thrusting because it is $\sim$ 4.4 meters thick versus average oolite thicknesses of about 2 meters in other sections in the southern Nopah Range [37, 59]. There is also less dramatic change in $\delta^{13}C$ from the bottom to the top of the oolite. The base of the oolite records $\delta^{13}C_{VPDB}$ values of -4.0‰ and decrease to -4.9‰ at the top (Fig. 3.5). There are approximately 10 meters of siltstone and orange carbonate-cemented sandstone between the oolite and pink limestones (Fig. 3.5). The sequence of pink limestones is thick ($\sim$ 20 meters) and includes intraclast and ooid grainstone with a variable number of grey limestone beds ($\sim$ 5–6) that contain crystal fan pseudomorphs (Fig. 3.4 and Fig. 3.5). The carbon isotopes in the pink limestone unit are more depleted in $\delta^{13}C_{VPDB}$ (-11.2‰) than in Johnson Canyon and become slightly less depleted in $\delta^{13}C_{VPDB}$ by the top of the pink limestones (-9.6‰) (Fig. 3.1).

3.5.5 Northern Mesquite Mountains (NM)

The upper Johnnie Formation in the northern Mesquite Mountains is thinner when compared to the Johnson Canyon and southern Nopah Range sections ($\sim$ 65 meters from the oolite to the Stirling contact), but carbonate lithologies comprise more of the preserved section (Fig. 3.5) [37]. The two sections of the oolite begin at -4.8‰ and -4.5‰ and become more $\delta^{13}C_{VPDB}$ -depleted up section, falling to -

6.0‰ and -5.5‰ (Fig. 3.6). The two sections agree well in excursion shape and magnitude for the first two meters. One section is thicker and $\delta^{13}C_{VPDB}$ continues to decline to -6.0 (Fig. 3.6). The limestone beds 13 meters above the oolite are thickly bedded pink ooid and intraclast grainstone with occasional small red chert nodules. $\delta^{13}C_{VPDB}$ analyses from these beds range from -10.9‰ to -9.9‰. The limestones are approximately 45 meters thick and disappear from the section close to the Stirling contact (Fig. 3.5) [37].

3.5.6 Salt Spring Hills (SS)

The Salt Spring Hills section of the Johnnie Formation is overall much thinner than the sections directly to the north, $\sim$ 250 meters versus 600 meters in the southern Nopah Range and 385 meters in the northern Mesquite Mountains [37]. The oolite $\delta^{13}C_{VPDB}$ composition in the Salt Spring Hills begins at -5.5‰ and -5.8‰ in the two sections sampled and falls to -6.0‰ and -6.9‰ at the top of the oolite (Fig. 3.6). The isotopic composition of the section that is more ^{13}C-depleted at the top (-6.9‰) shows more variability throughout the last meter of the oolite, and is also half a meter thicker (Fig. 3.6). There are no beds of pure carbonate above the oolite before the contact with the Stirling Quartzite but the section includes 12 meters of siltstones directly above the oolite and $\sim$ 25 meters of dolomite-cemented sandstone beds [37].

3.5.7 Old Dad Mountains (OD)

The southern-most section measured in this study is the most lithologically distinct. The entire section is only 165 meters thick, even thinner than the Salt Spring Hills section [37]. The Johnnie sits unconformably on gneissic basement, the older Pahrump Group strata are absent [36]. When mapping the lower sequences of the Johnnie, Summa (1993) noted that the first sequence is completely absent whereas the second sequence is thickened locally and dominantly carbonate, unlike other Death Valley sections. The Johnnie oolite at this section is extremely variable in thickness and can be locally surrounded by non-oolitic thickly laminated car-

bonates below and stromatolitic carbonates above [37]. Additionally, the isotopic range in δ^{13}C is the largest of any section. The two sections sampled are ∼30 meters from each other and yet the first oolite sampled (0.6 m thick) sits on top of siltstones and below a massive stromatolitic dolostone (1.6 meters thick) and the other oolite sampled (0.35 meters) is underlain by non-oolitic thickly laminated carbonates interbedded with siltstones (1.7 meters thick) and overlain by siltstones (Fig. 3.5). The $\delta^{13}C_{VPDB}$ at the base of the 0.6m oolite is -1.8‰ and the top of the oolite is -3.0‰. The massive carbonate directly overlying the oolite shows a continued decline from -3.9‰ to -5.1‰. A 20 cm carbonate bed ∼1 meter below the oolite was analyzed and $\delta^{13}C_{VPDB}$ falls from -1.3‰ to -1.6‰ over 15 cm. The $\delta^{13}C_{VPDB}$ of the laminated carbonates at the base of the second section begins at -1.4‰ and falls to -2.8‰. The overlying oolite shows a continued decline from -3.2‰ to -4.0‰ at the top of the oolite (Fig. 3.6). There are 65 meters of shale and siltstones preserved above the oolite, a pattern that is similar to the Rainstorm in the northern Spring Mountains and Resting Spring Range (Fig. 3.5). Directly below the base of the Stirling Formation, there are two massive cross-stratified carbonate grainstone beds (0.5 meters thick and 2 meters thick respectively) with shale in between the beds (Fig. 3.5). The $\delta^{13}C_{VPDB}$ composition from the one sample analyzed from the lower bed is -9.2‰. The three samples from the upper bed with increasing stratigraphic height are -7.5‰, -8.4‰ and -10.0‰.

3.6 Discussion

3.6.1 Petrographic and isotopic comparison across all sections

The depleted δ^{13}C and δ^{18}O data could be explained by either a primary marine signal, later diagenetic recrystallization and resetting, or a combination of the two. The preservation of primary textures can be an important indicator of the degree of diagenetic alteration and can begin to differentiate between these two mechanisms. Corsetti et al. (2006) completed a detailed analysis of the petrography and paragenesis of the Johnnie oolite using plane polarized light and cathodolumines-

cence. They found abundant evidence that the ooids underwent dolomitization very early in their history and that this transformation preserved much of the fine details of the original ooid fabrics and early marine cements. Some sections within their survey had evidence for later vadose zone cements and meteoric cements. These findings are consistent with our petrographic observations. Examples of ooids with well-preserved radial textures, individual cortices and detached cortices that were not destroyed by the surrounding cementation can be found in Fig. 3.4a, b. Some sections also include a poorly preserved end member characterized by micritized ooids and abundant fractures indicating further diagenetic modifications (Fig. 3.4c). The pink limestones overlying the oolite also show exceptionally preserved fabrics and record even more extreme δ^{13}C and δ^{18}O values. These textures include pseudomorphs of primary aragonite crystal fans that likely underwent stabilization to calcite very early in their history as well as extremely well-preserved radial ooids (Fig. 3.4d) [60].

Each section is characterized by declining δ^{13}C compositions with stratigraphic height and small first differences between samples. In contrast, the δ^{18}O values are highly variable with stratigraphic height and show no clear trend. The different character of the carbon and oxygen datasets suggest the oxygen isotopic compositions have been diagenetically reset while the possibility exists that the majority of the carbon isotopic compositions have not been reset. Pruss et al. (2008) micro sampled the crystal fan pseudomorphs in the pink limestones and found the different phases (fans versus early marine cements) to be isotopically indistinguishable [50]. Thus across several orders of magnitude in scale, the δ^{13}C data reveal a similar consistent pattern, despite being recorded in a wide range of fabrics that were differentially susceptible to fluid flow and diagenesis.

When aligned using the base of the oolite as a datum, the range in δ^{13}C of the different locations is striking (Fig. 3.7a). The $\delta^{13}C_{VPDB}$ at the base of the oolite ranges from -1.8‰ in the Old Dad Mountains to -5.8‰ in the Salt Spring Hills. The base of the oolite in the Old Dad Mountains is $\sim$ 1‰ heavier than the northern Spring Mountains and Resting Spring Range. The northern Spring

Mountains and Resting Spring Range oolites are $\sim 1‰$ heavier at the base than in Johnson Canyon, the southern Nopah Range and northern Mesquite Mountains. Finally, the northern Mesquite Mountains and southern Nopah Range are $\sim 1.5‰$ heavier than the base of the Salt Spring Hills oolite (Fig. 3.6). The top of the oolite records a range of values from -4.0‰ in the Old Dads to -6.9‰ in the Salt Spring Hills (Fig. 3.7a).

If the sections are aligned by their basal isotopic composition instead of by the stratigraphic datum and allowed to be mildly stretched or compressed (on the y-axis) to account for variable sedimentation rates through time, a general curve of changing isotopic composition emerges (Fig. 3.7b). Each section overlaps in $\delta^{13}C$ values with other sections. Rare single data points deviate from this curve in a few locations including the top of the southern Nopah Range section and the thicker of the two Salt Spring Hills sections indicating the isotopic record preserved in the thicker oolites could be complicated by structural folding and faulting (Fig. 3.7b).

Finally, despite clear evidence for fabric-retentive and fabric-destructive recrystallization in these rocks, $\delta^{13}C$ and $\delta^{18}O$ are not strongly correlated over the thickness of the oolite. This is distinct from several previous trends documented for large-magnitude negative $\delta^{13}C$ excursions elsewhere, and does not readily conform to the proposed diagenetic models [22, 23]. The six sections measured in the Salt Spring Hills, Johnson Canyon and northern Mesquite Mountains sections all define loose clusters in C-O space. In the Old Dad Mountains some of the most ^{18}O-depleted oxygen values correspond to the heaviest carbon values for both measured sections, which places them within the 'forbidden zone' outlined by Knauth and Kennedy (2009). This negative correlation in C-O isotope ratio space is opposite of expected diagenetic trends (Fig. 3.7c) [22, 23]. Some sections, however, do show a weak, but resolvable, positive correlation in C-O space, these include the southern Nopah Range, the northern Spring Mountains, and the Resting Spring Range. In each example, replicate sections differ in the strength (slope and residuals) of their covariance (Fig. 3.7c, Fig. 3.8). For both the Johnson Canyon and Southern Nopah sections $\delta^{18}O_{VPDB}$ values in the overlying pink limestone beds

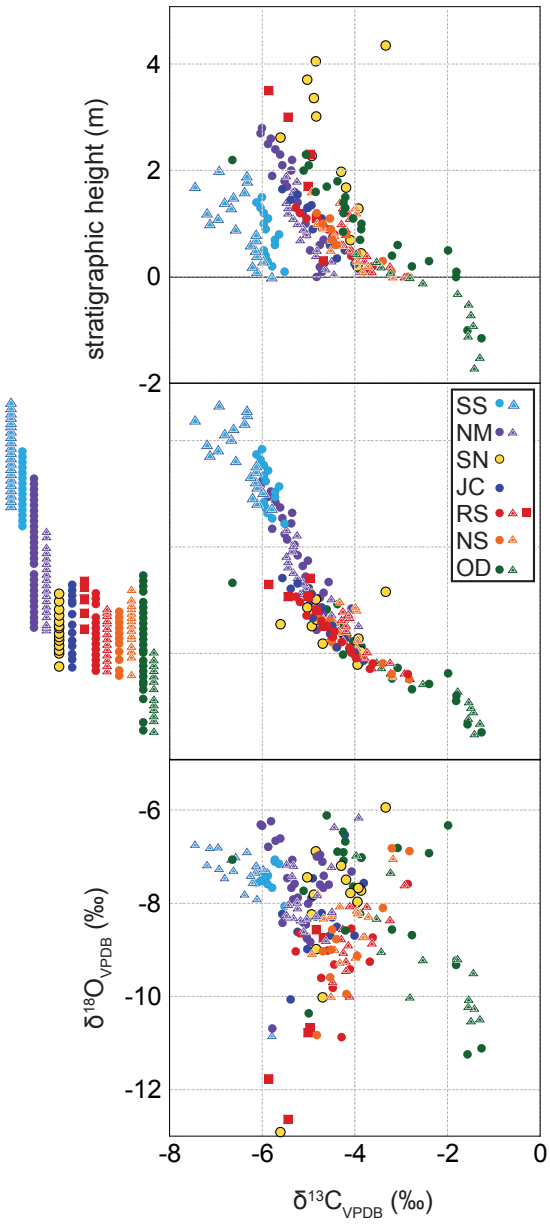

Figure 3.7: a) δ^{13}C data analyzed from all locations are aligned using the base of the Johnnie oolite as a datum. Aligned this way, at their base the data show a range of >4‰. b) The sections shifted on the y-axis based on their isotopic composition to create a composite curve. Shown alongside on the left, are the stratigraphic spacing adjustments required to produce the composite. Prior to the adjustments all sections were sampled at ∼10 cm intervals. c) A cross plot of δ^{13}C and δ^{18}O showing no discernible correlation between the two isotopic systems for SS, NM and JC sections. The SN, RS and NS sections show a clear, but weak, positive correlation while the OD section shows a negative relationship.

are exceedingly low (between -12‰ and -16‰).

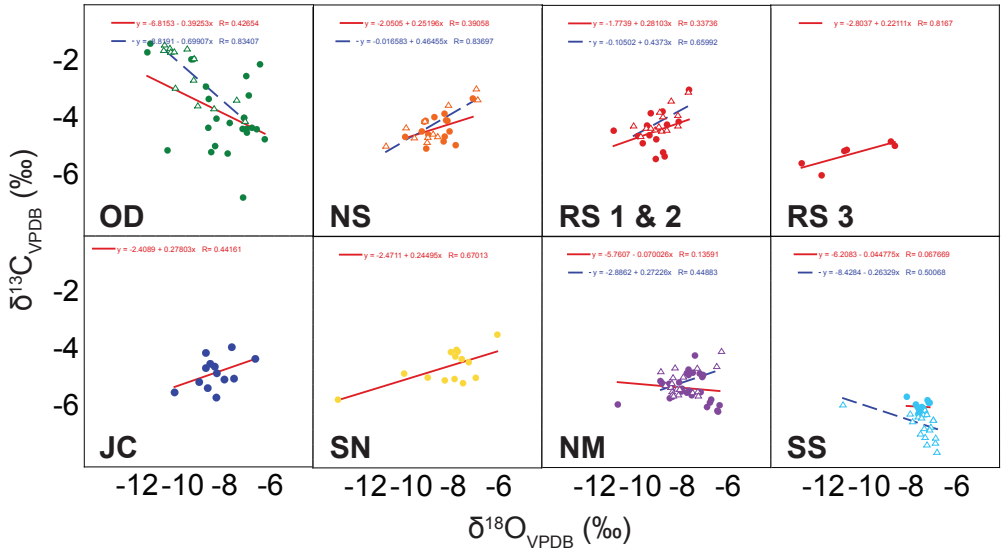

Figure 3.8: Cross plots of δ^{18}O and δ^{13}C for each section with linear fits and R^2 values. Old Dad Mountains (OD) is shown in green, northern Spring Mountains (NS) in orange, Resting Spring Range (RS) in red, Johnson Canyon (JC) in dark blue, southern Nopah Range (SN) is in yellow, northern Mesquite Mountains (NM) in purple, and Salt Spring Hills (SS) in light blue. The Resting Spring Range has three measured sections because the Johnnie oolite is structurally repeated in the section measured (RS 1, 2 and 3).

3.6.2 Isotopic results in the context of palinspastic reconstruction

Two periods of intense deformation in the Death Valley region have resulted in isolated exposures of the Johnnie Formation. Mesozoic crustal shortening and thin-skinned deformation resulted in several major thrust sequences that were oriented loosely parallel to the Laurentian margin, running north to south. Subsequent Cenozoic extension of the Basin and Range was oriented east-west and smeared out many of the pre-existing structures [61, 62].

To examine spatial patterns in the nature of the excursion observed in the Johnnie oolite, we used a palinspastic reconstruction of the central Basin and Range, constructed by Snow and Wernicke (2000) to un-do the Cenozoic extension. Their reconstruction relies on the reassembly of thrust fault exposures be-

tween the existing mountain ranges, regional facies and isopach correlations in the Death Valley region. Under this hypothesis, the key observation for reconstructing the Neoproterozoic sections rests on correlation of the Wheeler Pass thrust system in the Spring Mountains, the Chicago Pass thrust system in the northern Nopah Range and the Panamint thrust system in the Panamint Mountains [61]. This restores the Neoproterozoic sections to a thin north-south trending band that completely lies within the Wheeler Pass thrust sheet. From north to south the sections are as follows: northern Spring Mountain (NS), Resting Spring Range (RS), the Panamint Mountains Johnson Canyon (JC), southern Nopah Range (SN), northern Mesquite Mountains (NM), the Salt Spring Hills (SS) and Old Dad Mountains (OD)(Fig. 3.9). The Los Vegas Valley shear zone complicates the placement of the Old Dad Mountains within the reconstruction [61]. The Johnson Canyon section and the southern Nopah Range (SN) section restore to almost directly east-west of each other, an arrangement hypothesized by Stewart (1983) on the basis of offsets in both lithostratigraphy and isopach trends along the Furnace Creek fault system. In the reconstruction, the east-west distances preserved are small ($\sim$25 km) while there remains a large north-south distance between sections ($\sim$200 km) [61].

When the isotopic results are overlaid on the palinspastic reconstruction they exhibit a north-to-south trend within the Wheeler Pass thrust sheet with the exception of the Old Dad Mountains (Fig. 3.9). The basal composition of the oolite in the northernmost section is the least depleted while the southern Salt Spring Hills section is the most depleted. This pattern is consistent with the interpretation that the oolite is time transgressive and is recording a change in the isotopic composition of marine DIC. The carbonates preserved in the Old Dad Mountains would have been deposited first, while the northern Spring Mountains and Resting Spring Range would follow subsequently. The transgressing ooid shoals would reach the Salt Spring Hills last. Cessation of oolite deposition appears to follow a similar time-transgressive trend (Fig. 3.10). The sedimentology of the ooids (grain size and cross-stratification) reveals similar degrees of agitation and wave energy, it is very likely that the oolite was deposited under similar paleoenvironments and

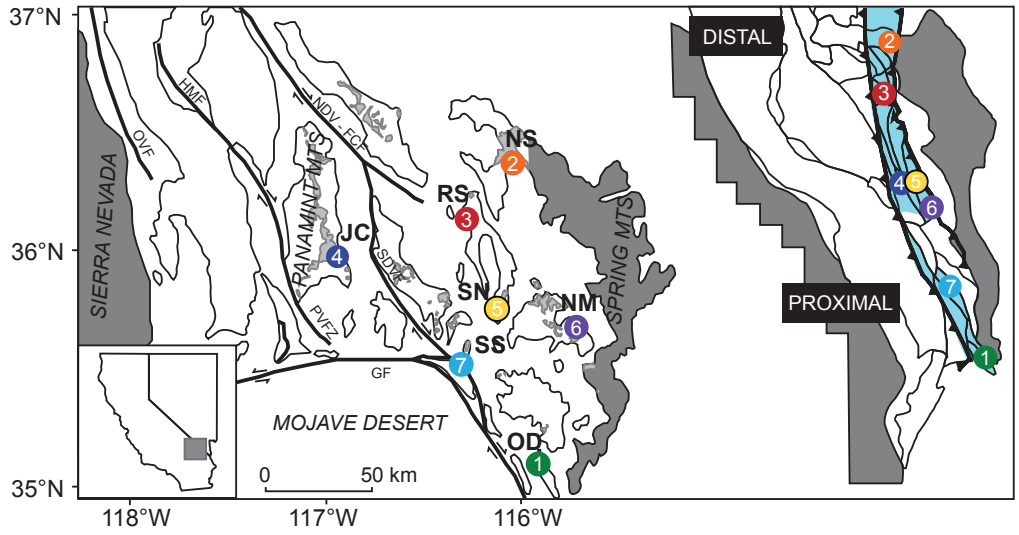

Figure 3.9: a) Current locations of the seven sampled sections of the Johnnie showing faults with significant displacement. The locations are the same as in Fig. 3.2 but ordinated with numbers indicating the degree of $\delta^{13}C$ depletion at the base of the oolite relative to the other locations, with one being the heaviest. Major Cenozoic faults are shown and labeled as Garlock Fault (GF), Panamint Valley Fault Zone (PVFZ), Owens Valley Fault (OVF), Hunter Mountain Fault (HMF) North Death Valley - Funeral Creek Fault (NDV - FCF), and South Death Valley Fault (SDVF) b) Palinspastic reconstruction accounting for Cenozoic extension aligns all locations in a north-to-south pattern within the Wheeler Pass thrust sheet.

Reconstruction using relationships from [61, 62].

water depths, and records the isotopic characteristics of a well-mixed water column and is not recording a gradient in the water column.

The north-to-south isotopic trend revealed by this analysis is interesting because it suggests different distal vs. proximal trends and paleoshoreline geometries than previous interpretations [36]. The shoreline to shelf direction has been interpreted as oriented (modern day) east to west with the paleoshoreline running north to south based on isopach maps, grain size trends and carbonate abundance within the overlying siliciclastic formations (i.e., Stirling Quartzite, Wood Canyon Formation and Zabriske Quartzite) [36]. The isotopic pattern on the other hand suggests the shelf direction to be north-south and the paleoshoreline to be more east-west. This interpretation matches the craton margin position (trending NE-SW) proposed by Fedo and Cooper [55].

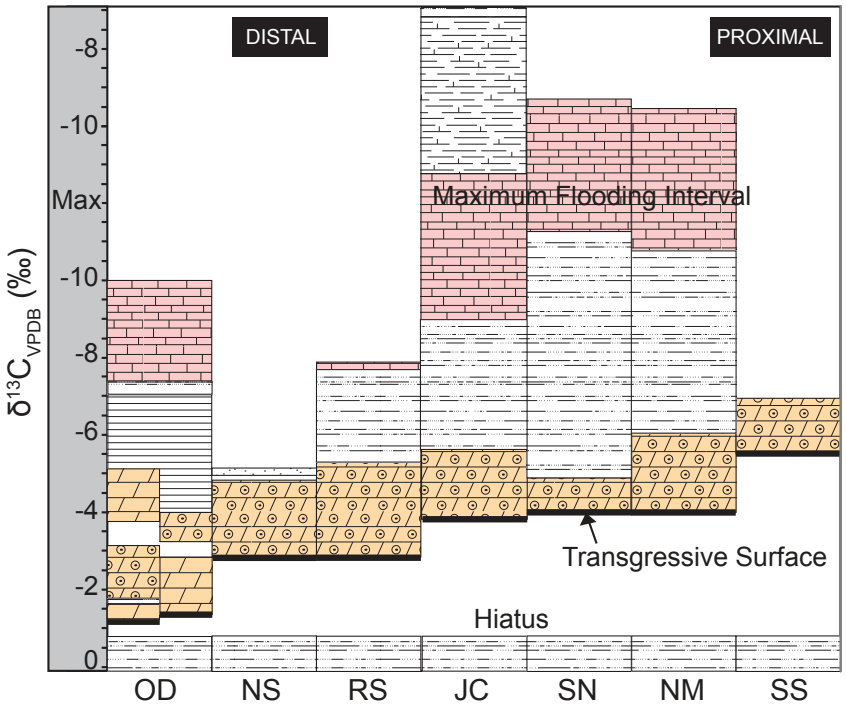

Figure 3.10: Chronostratigraphic diagram where isotopic composition is traded for relative time on the y-axis. The seven locations are ordered the same as in Fig. 3.9, with the heaviest δ^{13}C compositions at the base of the oolite on the left side of the diagram and the more depleted compositions on the right side of the diagram. The isotopic range in the overlying pink limestones is also shown for the locations where the observations exist. The isotopic scale for the pink limestones reflects whether the sections preserve the climbing limb of the excursion, the recovery or both.

Data from this study, [10, 11].

Additional sedimentologic evidence for this north-south distal-proximal interpretation includes isopach maps of the Johnnie Formation. Isopach data indicates both the Johnnie Formation and the thickness of the oolite to Stirling contact is thinnest in the southernmost sections—the northern Mesquite Mountains ($\sim$ 385 m thick Johnnie, $\sim$ 70 m thick oolite to Stirling), the Salt Spring Hills ($\sim$ 250 m, $\sim$ 45 m), the Silurian Hills ($\sim$ 115 m, $\sim$ 7 m), and the Old Dad Mountains ($\sim$ 165 m, $\sim$ 45m) [37]. The thickness and facies of the overlying pink limestones also suggest the northern sections are the most distal. In those sections the pink limestones are thin (10-20 cm thick) and micritic (Fig. 3.5) [37]. They are thickest in our proposed near shore sections—Johnson Canyon, southern Nopah Range and

northern Mesquite Mountains—where they sit between 5 and 15 meters above the oolite and are between 10 and 45 meters thick (Fig. 3.5) [37]. In these sections the pink limestones are mainly ooid and intraclast grainstones interpreted to represent storm deposits. In the Salt Spring Hills section, suggested by the isotopic data to be the most proximal, the pink limestone beds are missing entirely and are replaced by high-energy dolomite-cemented sandstone beds (Fig. 3.5). The unusual sedimentary structures, limestone composition and color (with precipitation of authigenic minerals) indicate that the pink limestone beds were probably deposited during an interval of maximum flooding following the transgression associated with the oolite deposition.

3.6.3 The Old Dad Mountains section is an outlier

The isotopic data for the Old Dad Mountains is not in line with the north-south trend seen across the other sections but its placement in the palinspastic reconstruction is the least constrained because of the Las Vegas Valley Shear Zone (LVVSZ). Both the isotopic data and sedimentology from the Old Dads suggest that the sediments might have been deposited in a tectonically isolated sub-basin (Fig. 3.5 and Fig. 3.6). The oolite in the Old Dads appears to be the first deposited as its basal isotopic composition is the least depleted in $\delta^{13}C$ (Fig. 3.5 and Fig. 3.6). The isotopic composition of the carbonates just below the Stirling contact suggest they were deposited at the same time or slightly earlier than the pink limestone facies in other locations even though there exists a substantial amount of intervening stratigraphy above the oolite in the Old Dad Mountains ($\sim$60 meters, in other sections this package is 5-30 meters) (Fig. 3.10).

Sedimentologically, the Old Dad Mountains are anomalous. The Johnnie Formation overlies crystalline quartzose gneissic basement, which is rare for the lower contact [37]. Additionally Summa (1993) identified two sequences within the lower Johnnie that also indicate the Old Dad Mountains might have been subject to unique basin dynamics. The lower most sequence of the Johnnie Formation is present in more northerly sections, thins to the east and is absent in the Salt Spring

Hills and Old Dad Mountains. The second sequence is also spatially variable and in the Old Dad Mountains it is one of the thickest exposures, and composed of pure carbonate unlike other sections suggesting that if a sub-basin existed this is when it became active [37]. The character of the Rainstorm Member is also unusual as the oolite is surrounded by thickly laminated carbonates and stromatolitic to massive carbonates as opposed to siltstone and shale lithologies (Fig. 3.5) [37]. The sedimentology and isotopic character of the Old Dad Mountains suggests very different sedimentation styles and rates compared to other sections supporting a model of an isolated sub-basin.

3.6.4 Could this sedimentary isotopic pattern represent a diagenetic signal?

There are two leading diagenetic hypotheses to explain large negative carbon isotopic excursions preserved in Neoproterozoic strata, but each invokes a set of diagenetic processes that are very different in their nature and respective timing [22, 23]. Oxygen isotope ratio data and observation of carbonate textures in these samples reveals clear evidence of post-depositional alteration. We can know with certainty that the chemistry of these rocks has been affected by recrystallization and re-equilibration with diagenetic fluids. However, petrographically these samples are well preserved, suggesting any such recrystallization occurred very early. The isotopic pattern within the Johnnie oolite and overlying pink limestones is neither uniform nor random across space, which is a challenging pattern to relate to known diagenetic processes. The spatial pattern observed can be used to test the robustness of these hypotheses for the origin of this carbon isotope excursion.

It is possible that our observed decline in the isotopic composition of the oolite and overlying carbonates could be produced by mixing with a plume of meteoric fluids moving through the oolite and overlying carbonates from nearshore sediments to more distal deposits (e.g., [23]). In that scenario, one would expect the nearshore environments and the more permeable sediments to be the most isotopically altered. The oolite is the most permeable carbonate-bearing lithology in

these sections. The Johnnie oolite presents the main fluid flow path for altering fluids, should have experienced higher water-to-rock ratios, and would therefore be predicted to have the most altered (^{13}C-depleted) isotopic composition. There is no doubt that the oolite was host to a variety of post-depositional fluids as evidenced by the variety of intragrain cements preserved within the oolite [63]. The overlying pink limestones, which include early-cemented crystal fans, should be less altered (more ^{13}C- and ^{18}O-enriched) than the oolite. The documented pattern shows exactly the opposite. Also according to this hypothesis [23], the Old Dad Mountains section should also reflect its cratonward location (more proximal to the source of altering fluids) and look similar to the Salt Spring Hills. Instead the oolite in the Old Dad Mountains has an isotopic composition that is the heaviest of all locations.

The burial diagenesis model proposed by Derry (2010), in which the isotopic composition reflects oxidation of organic matter from anomalously organic-rich Neoproterozoic rocks during deep burial, is difficult to rigorously assess in the Death Valley succession. These rocks present a challenge to look cleanly through the different episodes of deformation experienced by each of the different mountain ranges. However, there are a few observations in our data that bear on this hypothesis. As with other Ediacaran successions that record large negative excursions including the Shuram and Wonoka Formations, the rocks in the Rainstorm member of the Johnnie are organic lean today [1, 2, 10], and probably lacked a rich basinal source of hydrocarbons to provide high fCO_2, low δ^{13}C altering pore fluids. In addition, our results demonstrate that the isotopic signal preserved in the Johnnie oolite is systematic with stratigraphic height and systematically variable across the reconstructed Johnnie basin. Under this hypothesis we would expect the most depletion in the down dip (north) direction, again, this is opposite of the observed chemostratigraphic pattern. We should also expect that, as stated above, the alteration would have followed expected patterns of permeability and water-to-rock ratio, these are not observed. That in mind, it is possible that a clean diagenetic signal has been obscured by multiple episodes of diagenesis. Still, the

observation remains that these sections record a recognizable and repeatable signal across mountain ranges with different burial histories. This is consistent with the chemostratigraphic pattern being present in these rocks prior to Mesozoic time.

The systematic carbon isotopic variability observed in the Johnnie oolite does not appear to be well explained by existing diagenetic hypotheses. Within the oolite in each section the δ^{13}C composition becomes systematically heavier with stratigraphic height with small differences between adjacent samples. Across multiple sections tens of meters apart, the isotopic pattern is repeatable. Finally, a general north-to-south pattern of decreasing δ^{13}C is apparent across the Johnnie sedimentary basin. This isotopic pattern is consistent across orders of magnitude in length scale and lends support for the hypothesis that it captures elements of a primary isotopic signal. We therefore tentatively regard these carbon isotopic data as reflecting a trend in the isotopic composition of marine DIC.

3.7 Conclusions

Aspects of the geology and geochemistry of large-magnitude negative δ^{13}C anomalies expose fundamental issues in our ability to explain and understand chemostratigraphic patterns using uniform hypotheses. The results from this high-resolution study of the Johnnie oolite, which records the onset of one such negative excursion, add additional geologic constraints for future models. We demonstrate a systematic and reproducible stratigraphic pattern in the carbon isotope ratios of Rainstorm Member carbonates that aligns stratigraphic sections along a north-to-south gradient in a palinspastic reconstruction. These isotopic data fit the interpretation that deposition of the oolite was time transgressive. They also agree well with surrounding sedimentology and stratigraphy that suggest the northerly sections were more distal and the southerly sections were more proximal. The spatial pattern recorded in carbon isotope ratios is better explained by hypotheses whereby the oolite records time-series behavior of marine DIC, than hypotheses in which the δ^{13}C pattern is a result of post-depositional alteration. Though absolute

resolution of the problem remains currently out of reach, these results contribute to the growing list of geological observations that must be met by any satisfactory explanation of this large negative carbon isotope excursion.

3.8 Acknowledgements

We thank E. Trower, S. Finnegan, N. Boekelheide and E. Niedermeyer for assistance in the field. We also thank B. Wernicke, J. Grotzinger and M. Osburn for helpful discussions. Support was provided by the National Science Foundation through a Graduate Research Fellowship to K. Bergmann and by the Agouron Institute to W. Fischer for analytical support.

North Spring Mountains (NS) N 36°27'27.75" W 116°05'12.5" NAD27 CONUS			
stratigraphic height (m)	d13C	d18O	lithology
0.00	-3.18	-7.04	Dol. oolite
0.10	-3.83	-8.72	Dol. oolite
0.21	-3.71	-8.28	Dol. oolite
0.30	-3.96	-8.15	Dol. oolite
0.45	-3.94	-8.21	Dol. oolite
0.50	-4.52	-10.00	Dol. oolite
0.60	-4.33	-9.27	Dol. oolite
0.70	-4.51	-8.27	Dol. oolite
0.78	-4.44	-8.99	Dol. oolite
0.92	-4.68	-8.32	Dol. oolite
1.00	-4.81	-7.79	Dol. oolite
1.20	-3.96	-9.10	Dol. oolite
1.30	-3.99	-9.16	Dol. oolite
1.40	-4.33	-8.06	Dol. oolite
1.60	-4.93	-9.08	Dol. oolite
North Spring Mountains (NSa) N 36°27'29.1 W 116°05'11.7" NAD27 CONUS			
stratigraphic height (m)	d13C	d18O	lithology
0.00	-2.83	-6.88	Dol. oolite
0.10	-3.21	-6.82	Dol. oolite
0.30	-3.40	-8.10	Dol. oolite
0.45	-3.96	-9.13	Dol. oolite
0.60	-4.41	-8.77	Dol. oolite
0.70	-4.50	-8.57	Dol. oolite
0.80	-4.19	-9.95	Dol. oolite
0.90	-4.52	-9.00	Dol. oolite
1.00	-4.70	-9.03	Dol. oolite
1.10	-4.54	-9.59	Dol. oolite
1.20	-4.83	-10.83	Dol. oolite
Resting Spring Range (RS) N 36°09'17.8" W 116°14'11.4" NAD27 CONUS			
stratigraphic height (m)	d13C	d18O	lithology
0.00	-2.86	-7.58	Dol. oolite
0.10	-3.68	-9.25	Dol. oolite
0.20	-3.62	-8.73	Dol. oolite
0.30	-3.98	-8.03	Dol. oolite
0.40	-4.08	-8.54	Dol. oolite
0.50	-4.11	-9.41	Dol. oolite
0.60	-4.29	-10.87	Dol. oolite

Table 3.1: Isotopic data and location coordinates for each stratigraphic section sampled. Most locations have multiple sections, collected to assay reproducibility along strike (i.e. NM and NMa). Data is reported referenced to VPDB. Location coordinates are referenced to the NAD27 CONUS datum. All of the Johnnie oolite data is reported as Dol. oolite in the lithology column for dolomitic oolite. Additional data for the overlying limestones is reported for sections where samples were taken.

Resting Spring Range (RS) cont'd N 36°09'17.8" W 116°14'11.4" NAD27 CONUS			
stratigraphic height (m)	d13C	d18O	lithology
0.70	-4.48	-9.81	Dol. oolite
0.80	-4.45	-9.31	Dol. oolite
0.90	-4.59	-9.01	Dol. oolite
1.00	-4.73	-9.60	Dol. oolite
1.10	-5.05	-8.71	Dol. oolite
1.20	-5.19	-8.64	Dol. oolite
1.30	-5.28	-9.03	Dol. oolite
Resting Spring Range (RSa) N 36°09'19.4" W 116°14'08.9" NAD27 CONUS			
stratigraphic height (m)	d13C	d18O	lithology
0.00	-2.93	-7.60	Dol. oolite
0.10	-3.63	-8.85	Dol. oolite
0.20	-3.24	-8.35	Dol. oolite
0.30	-3.79	-8.71	Dol. oolite
0.40	-3.74	-8.06	Dol. oolite
0.50	-4.11	-8.05	Dol. oolite
0.60	-4.25	-9.05	Dol. oolite
0.70	-4.48	-9.68	Dol. oolite
0.80	-4.19	-9.44	Dol. oolite
0.90	-4.19	-9.24	Dol. oolite
1.00	-4.29	-8.76	Dol. oolite
1.10	-4.11	-9.99	Dol. oolite
1.20	-4.14	-8.89	Dol. oolite
1.30	-4.26	-8.54	Dol. oolite
Resting Spring Range (RSMc) N 36°09'17.7" W 116°14'04.2"			
stratigraphic height (m)	d13C	d18O	lithology
0.30	-4.68	-8.74	Dol. oolite
1.10	-4.83	-8.57	Dol. oolite
1.70	-5.01	-10.78	Dol. oolite
2.30	-4.97	-10.67	Dol. oolite
3.00	-5.44	-12.64	Dol. oolite
3.50	-5.86	-11.77	Dol. oolite
6.50	-7.96	-16.54	pink micritic limestone

Table 3.2: Isotopic data and location coordinates for each stratigraphic section sampled. Most locations have multiple sections, collected to assay reproducibility along strike (i.e. NM and NMa). Data is reported referenced to VPDB. Location coordinates are referenced to the NAD27 CONUS datum. All of the Johnnie oolite data is reported as Dol. oolite in the lithology column for dolomitic oolite. Additional data for the overlying limestones is reported for sections where samples were taken.

Southern Nopahs (SN) N 36°49'34.2" W 116°4'48.0" NAD27 CONUS			
stratigraphic height (m)	d13C	d18O	lithology
0.20	-3.95	-7.97	Dol. oolite
0.44	-3.87	-7.72	Dol. oolite
0.69	-4.10	-7.78	Dol. oolite
0.94	-4.70	-10.02	Dol. oolite
1.29	-3.93	-7.67	Dol. oolite
1.68	-4.19	-7.49	Dol. oolite
1.98	-4.30	-7.19	Dol. oolite
2.27	-4.93	-8.23	Dol. oolite
2.62	-5.61	-12.91	Dol. oolite
3.02	-4.84	-8.98	Dol. oolite
3.36	-4.89	-7.81	Dol. oolite
3.71	-5.03	-7.44	Dol. oolite
4.05	-4.85	-6.88	Dol. oolite
4.35	-3.34	-5.94	Dol. oolite
14.43	-11.22	-15.73	pink micritic limestone
14.63	-11.10	-15.00	pink micritic limestone
14.76	-11.13	-15.53	pink micritic limestone
14.97	-10.53	-15.58	pink micritic limestone
15.17	-11.12	-15.85	pink micritic limestone
15.32	-11.29	-15.66	pink micritic limestone
15.52	-11.16	-14.91	pink micritic limestone
15.76	-10.19	-13.97	pink micritic limestone
16.06	-10.54	-15.20	pink micritic limestone
16.26	-11.39	-15.78	pink micritic limestone
17.44	-11.28	-15.39	pink micritic limestone
17.83	-11.47	-15.33	pink micritic limestone
18.03	-11.75	-15.70	pink micritic limestone
18.42	-11.42	-15.98	pink micritic limestone
20.04	-11.18	-15.58	pink micritic limestone
20.58	-10.90	-15.52	pink micritic limestone
21.15	-10.42	-15.95	pink micritic limestone
21.38	-10.50	-15.20	pink micritic limestone
21.58	-11.36	-15.64	pink micritic limestone
22.08	-11.35	-15.80	pink micritic limestone
23.08	-9.77	-15.44	pink micritic limestone
23.28	-11.19	-15.58	pink micritic limestone
24.78	-11.21	-15.58	intrclast congl.
25.78	-10.95	-15.68	pink micritic limestone
26.08	-11.06	-15.37	pink micritic limestone
26.93	-11.26	-15.632224	pink micritic limestone
27.42	-10.55	-15.051862	pink micritic limestone
27.67	-10.69	-15.079304	pink micritic limestone
28.07	-10.91	-15.479842	pink micritic limestone

Table 3.3: Isotopic data and location coordinates for each stratigraphic section sampled. Most locations have multiple sections, collected to assay reproducibility along strike (i.e. NM and NMa). Data is reported referenced to VPDB. Location coordinates are referenced to the NAD27 CONUS datum. All of the Johnnie oolite data is reported as Dol. oolite in the lithology column for dolomitic oolite. Additional data for the overlying limestones is reported for sections where samples were taken.

Southern Nopahs (SN) cont'd			
stratigraphic height (m)	d13C	d18O	lithology
28.41	-10.47	-14.835372	grey crystal fans
28.87	-10.73	-15.2155	pink micritic limestone
29.32	-9.87	-14.885174	intraclast congl.
31.22	-9.72	-14.798133	grey crystal fans
32.02	-10.49	-15.637236	pink micritic limestone
32.47	-9.69	-15.005108	pink micritic limestone
33.76	-10.21	-16.106914	pink micritic limestone
Johnson Canyon (JC) 36°4'55" N, 116°58'14" W NAD27 CONUS			
* this is from C. Verdel -- did you take a waypoint?			
stratigraphic height (m)	d13C	d18O	Lithology
0.10	-3.81	-7.56	Dol. oolite
0.25	-4.01	-8.69	Dol. oolite
0.35	-4.39	-8.50	Dol. oolite
0.50	-4.22	-6.53	Dol. oolite
0.60	-4.54	-8.69	Dol. oolite
0.75	-4.49	-8.30	Dol. oolite
0.90	-4.91	-7.46	Dol. oolite
1.10	-4.72	-8.21	Dol. oolite
1.30	-5.03	-8.98	Dol. oolite
1.35	-4.94	-7.88	Dol. oolite
1.45	-5.39	-10.06	Dol. oolite
1.55	-5.24	-8.61	Dol. oolite
1.65	-5.57	-8.23	Dol. oolite
8.00	-8.55	-12.36	pink limestone
9.00	-8.61	-15.45	pink limestone
10.00	-9.00	-12.80	pink limestone
11.00	-10.40	-11.36	pink limestone
13.00	-10.50	-14.73	pink limestone
15.00	-11.01	-15.91	pink limestone

Table 3.4: Isotopic data and location coordinates for each stratigraphic section sampled. Most locations have multiple sections, collected to assay reproducibility along strike (i.e. NM and NMa). Data is reported referenced to VPDB. Location coordinates are referenced to the NAD27 CONUS datum. All of the Johnnie oolite data is reported as Dol. oolite in the lithology column for dolomitic oolite. Additional data for the overlying limestones is reported for sections where samples were taken.

North Mesquite Mountains (NM) N 35°46'09.6" W 115°44'38.5" NAD27 CONUS			
stratigraphic height (m)	d13C	d18O	lithology
0.00	-4.83	-7.00	Dol. oolite
0.10	-4.71	-7.11	Dol. oolite
0.19	-4.76	-7.60	Dol. oolite
0.29	-4.69	-7.67	Dol. oolite
0.40	-4.08	-7.32	Dol. oolite
0.50	-4.97	-8.83	Dol. oolite
0.60	-4.76	-6.96	Dol. oolite
0.70	-4.68	-7.41	Dol. oolite
0.80	-5.04	-8.76	Dol. oolite
0.90	-4.57	-7.60	Dol. oolite
1.00	-5.07	-8.45	Dol. oolite
1.20	-5.13	-8.41	Dol. oolite
1.30	-5.02	-8.01	Dol. oolite
1.40	-5.24	-7.88	Dol. oolite
1.50	-5.34	-7.92	Dol. oolite
1.60	-5.31	-7.58	Dol. oolite
1.70	-5.47	-7.46	Dol. oolite
1.80	-5.52	-8.30	Dol. oolite
1.90	-5.79	-10.69	Dol. oolite
2.00	-5.38	-7.67	Dol. oolite
2.10	-5.57	-8.42	Dol. oolite
2.20	-5.36	-7.07	Dol. oolite
2.30	-5.62	-6.61	Dol. oolite
2.40	-5.72	-6.66	Dol. oolite
2.50	-5.88	-6.79	Dol. oolite
2.60	-5.82	-6.24	Dol. oolite
2.70	-6.04	-6.31	Dol. oolite
2.80	-6.01	-6.34	Dol. oolite
30.00	-10.87	-8.23	pink oolitic limestone
48.00	-9.90	-8.95	pink oolitic limestone
North Mesquite Mountains (NMa) N 35°46'11.7" W 115°44'38.0" NAD27 CONUS			
stratigraphic height (m)	d13C	d18O	lithology
0.05	-4.45	-6.36	Dol. oolite
0.10	-3.92	-6.15	Dol. oolite
0.15	-4.63	-8.80	Dol. oolite
0.30	-4.50	-8.18	Dol. oolite
0.40	-4.84	-8.27	Dol. oolite
0.50	-4.82	-7.82	Dol. oolite
0.60	-4.51	-7.21	Dol. oolite
0.70	-5.18	-8.36	Dol. oolite

Table 3.5: Isotopic data and location coordinates for each stratigraphic section sampled. Most locations have multiple sections, collected to assay reproducibility along strike (i.e. NM and NMa). Data is reported referenced to VPDB. Location coordinates are referenced to the NAD27 CONUS datum. All of the Johnnie oolite data is reported as Dol. oolite in the lithology column for dolomitic oolite. Additional data for the overlying limestones is reported for sections where samples were taken.

North Mesquite Mountains (NMa) cont'd N 35°46'11.7" W 115°44'38.0" NAD27 CONUS			
stratigraphic height (m)	d13C	d18O	lithology
0.80	-5.04	-8.32	Dol. oolite
0.90	-5.11	-8.60	Dol. oolite
1.00	-5.24	-8.10	Dol. oolite
1.10	-5.33	-8.31	Dol. oolite
1.20	-5.44	-8.03	Dol. oolite
1.30	-5.44	-8.30	Dol. oolite
1.40	-5.48	-8.25	Dol. oolite
1.50	-5.36	-7.41	Dol. oolite
1.60	-5.33	-7.19	Dol. oolite
1.80	-5.25	-7.98	Dol. oolite
1.90	-5.48	-7.16	Dol. oolite
Salt Spring Hills (SS) N 35°35'42.3" W 116°16'20.9" NAD27 CONUS			
stratigraphic height (m)	d13C	d18O	lithology
0.10	-5.52	-8.06	Dol. oolite
0.20	-5.79	-7.66	Dol. oolite
0.30	-5.89	-7.58	Dol. oolite
0.40	-5.93	-7.45	Dol. oolite
0.50	-5.97	-7.48	Dol. oolite
0.60	-5.73	-7.10	Dol. oolite
0.70	-5.73	-7.06	Dol. oolite
0.80	-5.64	-7.15	Dol. oolite
0.90	-5.93	-7.33	Dol. oolite
1.00	-5.97	-7.49	Dol. oolite
1.10	-5.88	-7.40	Dol. oolite
1.20	-5.97	-7.42	Dol. oolite
1.30	-6.04	-7.52	Dol. oolite
1.40	-6.13	-7.56	Dol. oolite
1.50	-6.01	-7.30	Dol. oolite
Salt Spring Hills (SSa) N 35deg35'40.8" W 116deg16'20.6" NAD27 CONUS			
stratigraphic height (m)	d13C	d18O	lithology
0.00	-5.79	-10.84	Dol. oolite
0.10	-6.11	-7.90	Dol. oolite
0.20	-6.21	-7.55	Dol. oolite
0.30	-5.98	-7.26	Dol. oolite
0.40	-6.11	-7.20	Dol. oolite
0.50	-6.14	-7.33	Dol. oolite
0.60	-6.25	-7.40	Dol. oolite

Table 3.6: Isotopic data and location coordinates for each stratigraphic section sampled. Most locations have multiple sections, collected to assay reproducibility along strike (i.e. NM and NMa). Data is reported referenced to VPDB. Location coordinates are referenced to the NAD27 CONUS datum. All of the Johnnie oolite data is reported as Dol. oolite in the lithology column for dolomitic oolite. Additional data for the overlying limestones is reported for sections where samples were taken.

Salt Spring Hills (SSa) cont'd N 35°35'40.8" W 116°16'20.6" NAD27 CONUS			
0.70	-6.13	-7.18	Dol. oolite
0.80	-6.13	-7.18	Dol. oolite
0.90	-6.57	-7.00	Dol. oolite
1.00	-7.13	-6.80	Dol. oolite
1.10	-6.95	-6.79	Dol. oolite
1.20	-7.19	-7.17	Dol. oolite
1.30	-6.67	-7.05	Dol. oolite
1.40	-6.81	-7.45	Dol. oolite
1.50	-6.62	-7.29	Dol. oolite
1.60	-6.38	-7.80	Dol. oolite
1.70	-7.45	-6.73	Dol. oolite
1.80	-6.32	-6.89	Dol. oolite
1.90	-6.33	-6.89	Dol. oolite
2.00	-6.93	-7.25	Dol. oolite
Old Dad Mountains (OD) N 35°10'47.1" W 115°52'57.9" NAD27 CONUS			
stratigraphic height (m)	d13C	d18O	lithology
-1.15	-1.27	-11.11	massive dolstne
-1.00	-1.57	-11.24	massive dolstne
0.00	-1.82	-9.32	laminated dolstne
0.10	-1.81	-9.22	Dol. oolite
0.20	-2.77	-8.68	Dol. oolite
0.30	-2.40	-6.92	Dol. oolite
0.40	-3.20	-8.56	Dol. oolite
0.50	-1.99	-6.32	Dol. oolite
0.60	-3.08	-6.81	Dol. oolite
0.70	-3.89	-8.22	massive dolstne
0.85	-4.26	-6.46	massive dolstne
0.90	-3.87	-7.02	massive dolstne
1.00	-3.86	-7.01	massive dolstne
1.10	-4.04	-7.64	massive dolstne
1.20	-4.25	-7.08	massive dolstne
1.30	-4.21	-6.67	massive dolstne
1.40	-4.25	-6.90	massive dolstne
1.50	-4.21	-8.58	massive dolstne
1.60	-4.85	-8.28	massive dolstne
1.70	-4.61	-6.11	massive dolstne
1.80	-4.38	-6.89	massive dolstne
2.00	-5.11	-7.73	massive dolstne
2.10	-5.00	-10.36	massive dolstne
2.20	-6.65	-7.06	massive dolstne
2.30	-5.06	-8.45	massive dolstne
67.75	-9.20	-6.76	x-bedded grainstone

Table 3.7: Isotopic data and location coordinates for each stratigraphic section sampled. Most locations have multiple sections, collected to assay reproducibility along strike (i.e. NM and NMa). Data is reported referenced to VPDB. Location coordinates are referenced to the NAD27 CONUS datum. All of the Johnnie oolite data is reported as Dol. oolite in the lithology column for dolomitic oolite. Additional data for the overlying limestones is reported for sections where samples were taken.

Old Dad Mountains (OD) cont'd N 35°10'47.1" W 115°52'57.9" NAD27 CONUS			
stratigraphic height (m)	d13C	d18O	lithology
69.75	-7.52	-2.40	x-bedded grainstone
70.50	-8.36	-5.46	x-bedded grainstone
71.50	-10.06	-6.12	x-bedded grainstone
Old Dad Mountains (ODa) N 35°10'47.5" W 115°52'54.2" NAD27 CONUS			
stratigraphic height (m)	d13C	d18O	lithology
0.00	-1.42	-10.25	laminated dolstne
0.20	-1.30	-10.48	laminated dolstne
0.60	-1.55	-10.21	laminated dolstne
0.80	-1.44	-9.49	laminated dolstne
1.00	-1.49	-10.52	laminated dolstne
1.20	-1.54	-10.06	laminated dolstne
1.40	-1.78	-9.19	laminated dolstne
1.60	-2.53	-9.21	laminated dolstne
1.70	-2.81	-10.01	laminated dolstne
1.80	-3.23	-7.33	Dol. oolite
1.90	-3.43	-9.03	Dol. oolite
2.00	-3.53	-8.32	Dol. oolite
2.15	-3.97	-6.96	Dol. oolite

Table 3.8: Isotopic data and location coordinates for each stratigraphic section sampled. Most locations have multiple sections, collected to assay reproducibility along strike (i.e. NM and NMa). Data is reported referenced to VPDB. Location coordinates are referenced to the NAD27 CONUS datum. All of the Johnnie oolite data is reported as Dol. oolite in the lithology column for dolomitic oolite. Additional data for the overlying limestones is reported for sections where samples were taken.

References

[1] C.R. Calver. Isotope stratigraphy of the Ediacaran (Neoproterozoic III) of the Adelaide Rift Complex, Australia, and the overprint of water column stratification. *Precambrian Research*, 100(1-3):121–150, 2000.

[2] D.A. Fike, J.P. Grotzinger, L.M. Pratt, and R.E. Summons. Oxidation of the Ediacaran ocean. *Nature*, 444(7120):744–747, 2006.

[3] G.Q. Jiang, A.J. Kaufman, N. Christie-Blick, S.H. Zhang, and H.C. Wu. Carbon isotope variability across the Ediacaran Yangtze platform in South China: Implications for a large surface-to-deep ocean delta C-13 gradient. *Earth and Planetary Science Letters*, 261(1-2):303–320, 2007.

[4] V.A. Melezhik, A.E. Fallick, and B.G. Pokrovsky. Enigmatic nature of thick sedimentary carbonates depleted in C-13 beyond the canonical mantle value: The challenges to our understanding of the terrestrial carbon cycle. *Precambrian Research*, 137(3-4):131–165, 2005.

[5] S.J. Burns and A. Matter. Carbon isotopic record of the latest Proterozoic from Oman. *Eclogae Geologicae Helvetiae*, 86(2):595–607, 1993.

[6] E. Le Guerroue, P.A. Allen, A. Cozzi, J.L. Etienne, and M. Fanning. 50 myr recovery from the largest negative delta C-13 excursion in the Ediacaran ocean. *Terra Nova*, 18(2):147–153, 2006.

[7] G.M.E. McCarron. *The sedimentology and chemostratigraphy of the Nafun Group, Huqf Supergroup, Oman.* Ph.D. thesis, 2000.

[8] K.A. McFadden, J. Huang, X.L. Chu, G.Q. Jiang, A.J. Kaufman, C.M. Zhou, X.L. Yuan, and S.H. Xiao. Pulsed oxidation and biological evolution in the Ediacaran Doushantuo Formation. *Proceedings of the National Academy of Sciences of the United States of America*, 105(9):3197–3202, 2008.

[9] F.A. Corsetti and A.J. Kaufman. Stratigraphic investigations of carbon isotope anomalies and Neoproterozoic ice ages in Death Valley, California. *Geological Society of America Bulletin*, 115(8):916–932, 2003.

[10] A.J. Kaufman, F.A. Corsetti, and M.A. Varni. The effect of rising atmospheric oxygen on carbon and sulfur isotope anomalies in the Neoproterozoic Johnnie Formation, Death Valley, USA. *Chemical Geology*, 237(1-2):47–63, 2007.

[11] C. Verdel, B.P. Wernicke, and S.A. Bowring. The Shuram and subsequent Ediacaran carbon isotope excursions from southwest Laurentia, and implications for environmental stability during the metazoan radiation. *Geological Society of America Bulletin*, 123(7/8):1539–1559, 2011.

[12] V.A. Melezhik, B.G. Pokrovsky, A.E. Fallick, A.B. Kuznetsov, and M.I. Bujakaite. Constraints on Sr-87/Sr-86 of Late Ediacaran seawater: insight from Siberian high-Sr limestones. *Journal of the Geological Society*, 166:183–191, 2009.

[13] J.B. Ries, D.A. Fike, L.M. Pratt, T.W. Lyons, and J.P. Grotzinger. Superheavy pyrite (delta S-34(pyr) ¿ delta S-34(CAS)) in the terminal Proterozoic Nama Group, southern Namibia: A consequence of low seawater sulfate at the dawn of animal life. *Geology*, 37(8):743–746, 2009.

[14] B.Z. Saylor, A.J. Kaufman, J.P. Grotzinger, and F. Urban. A composite reference section for terminal Proterozoic strata of southern Namibia. *Journal of Sedimentary Research*, 68(6):1223–1235, 1998.

[15] V.A. Melezhik, D. Roberts, A.E. Fallick, and I.M. Gorokhov. The Shuram-Wonoka event recorded in a high-grade metamorphic terrane: Insight from the Scandinavian Caledonides. *Geological Magazine*, 145(2):161–172, 2008.

[16] A.R. Prave, R.A. Strachan, and A.E. Fallick. Global C cycle perturbations recorded in marbles: a record of Neoproterozoic Earth history within the Dalradian succession of the Shetland Islands, Scotland. *Journal of the Geological Society*, 166:129–135, 2009.

[17] D. Condon, M.Y. Zhu, S. Bowring, W. Wang, A.H. Yang, and Y.G. Jin. U-Pb ages from the Neoproterozoic Doushantuo Formation, China. *Science*, 308(5718):95–98, 2005.

[18] S.A. Bowring, J.P. Grotzinger, D.J. Condon, J. Ramezani, M.J. Newall, and P.A. Allen. Geochronologic constraints on the chronostratigraphic framework of the Neoproterozoic Huqf Supergroup, Sultanate of Oman. *American Journal of Science*, 307(10):1097–1145, 2007.

[19] J.P. Grotzinger, S.A. Bowring, B.Z. Saylor, and A.J. Kaufman. Biostratigraphic and geochronological constraints on early animal evolution. *Science*, 270(5236):598–604, 1995.

[20] L.R. Kump. Interpreting carbon-isotope excursions - strangelove oceans. *Geology*, 19(4):299–302, 1991.

[21] D.H. Rothman, J.M. Hayes, and R.E. Summons. Dynamics of the Neoproterozoic carbon cycle. *Proceedings of the National Academy of Sciences of the United States of America*, 100(14):8124–8129, 2003.

[22] L.A. Derry. A burial diagenesis origin for the Ediacaran Shuram-Wonoka carbon isotope anomaly. *Earth and Planetary Science Letters*, 294(1-2):152–162, 2010.

[23] L.P. Knauth and M.J. Kennedy. The late Precambrian greening of the Earth. *Nature*, 460(7256):728–732, 2009.

[24] E. Le Guerroue, P.A. Allen, and A. Cozzi. Chemostratigraphic and sedimentological framework of the largest negative carbon isotopic excursion in Earth

history: The Neoproterozoic Shuram Formation (Nafun Group, Oman). *Precambrian Research*, 146(1-2):68–92, 2006.

[25] E. Le Guerroue. Duration and synchroneity of the largest negative carbon isotope excursion on Earth: The Shuram/Wonoka anomaly. *Comptes Rendus Geoscience*, 342(3):204–214, 2010.

[26] D.E. Canfield, S.W. Poulton, and G.M. Narbonne. Late-Neoproterozoic deep-ocean oxygenation and the rise of animal life. *Science*, 315(5808):92–95, 2007.

[27] A.L. Cohen and M. Holcomb. Why corals care about ocean acidification: Uncovering the mechanism. *Oceanography*, 22(4):118–127, 2009.

[28] G.P. Halverson, P.F. Hoffman, D.P. Schrag, and A.J. Kaufman. A major perturbation of the carbon cycle before the Ghaub glaciation (Neoproterozoic) in Namibia: Prelude to snowball Earth? *Geochemistry Geophysics Geosystems*, 3:–, 2002.

[29] E.A. Sperling and K.J. Peterson. Poriferan paraphyly and its implications for Precambrian paleobiology. *Integrative and Comparative Biology*, 46:E134–E134, 2006.

[30] T.F. Bristow and M.J. Kennedy. Carbon isotope excursions and the oxidant budget of the Ediacaran atmosphere and ocean. *Geology*, 36(11):863–866, 2008.

[31] P.K. Swart. Global synchronous changes in the carbon isotopic composition of carbonate sediments unrelated to changes in the global carbon cycle. *Proceedings of the National Academy of Sciences of the United States of America*, 105(37):13741–13745, 2008.

[32] G.P. Halverson, P.F. Hoffman, D.P. Schrag, A.C. Maloof, and A.H.N. Rice. Toward a Neoproterozoic composite carbon-isotope record. *Geological Society of America Bulletin*, 117(9-10):1181–1207, 2005.

[33] G.P. Halverson, B.P. Wade, M.T. Hurtgen, and K.M. Barovich. Neoproterozoic chemostratigraphy. *Precambrian Research*, 182(4):337–350, 2010.

[34] F.A. Macdonald, D.S. Jones, and D.P. Schrag. Stratigraphic and tectonic implications of a newly discovered glacial diamictite-cap carbonate couplet in southwestern Mongolia. *Geology*, 37(2):123–126, 2009.

[35] C. Verdel. *I. Cenozoic geology of Iran: an integrated study of extensional tectonics and related volcanism II. Ediacaran stratigraphy of the North American Cordillera: new observations from eastern California and northern Utah.* Ph.D. thesis, 2009.

[36] J.H. Stewart. Upper Precambrian and lower Cambrian strata in the southern Great Basin, California and Nevada, 1970.

[37] C. Summa. *Sedimentologic, stratigraphic, and tectonic controls of a mixed carbonate-siliciclastic succession: Neoproterozoic Johnnie Formation, southeast California.* Ph.D. thesis, 1993.

[38] P.F. Hoffman, G.P. Halverson, E.W. Domack, J.M. Husson, J.A. Higgins, and D.P. Schrag. Are basal Ediacaran (635 Ma) post-glacial "cap dolostones" diachronous? *Earth and Planetary Science Letters*, 258(1-2):114–131, 2007.

[39] D.S. Jones, D.A. Fike, S. Finnegan, W.W. Fischer, and D.P. Schrag. Terminal Ordovician carbon isotope stratigraphy and glacioeustatic sea-level change across Anticosti Island (Quebec, Canada). *Geological Society of America Bulletin*, 123(7/8):1645–1644, 2011.

[40] A.R. Prave. Two diamictites, two cap carbonates, two delta C-13 excursions, two rifts: The Neoproterozoic Kingston Peak Formation, Death Valley, California. *Geology*, 27(4):339–342, 1999.

[41] M.J. Abolins. *I. Stratigraphic constraints on the number of discrete Neoproterozoic glaciations and the relationship between glaciation and Ediacaran evolution. II. The Kwichup Spring thrust in the northwestern Spring Mountains,*

Nevada: implications for large-magnitude extension and the structure of the Cordilleran thrust belt. Ph.D. thesis, 1999.

[42] T.C. Labotka, A.L. Albee, M.A. Lanphere, and S.D. Mcdowell. Stratigraphy, structure, and metamorphism in the central Panamint Mountains (Telescope-Peak Quadrangle), Death-Valley area, California - summary. *Geological Society of America Bulletin*, 91(3):125–129, 1980.

[43] L.M. Heaman and J.P. Grotzinger. 1.08 Ga diabase sills in the Pahrump Group, California - implications for development of the Cordilleran Miogeocline. *Geology*, 20(7):637–640, 1992.

[44] F.A. Corsetti, J.H. Stewart, and J.W. Hagadorn. Neoproterozoic diamictite-cap carbonate succession and delta C-13 chemostratigraphy from eastern Sonora, Mexico. *Chemical Geology*, 237(1-2):129–142, 2007.

[45] F.A. Corsetti, A. Baud, P.J. Marenco, and S. Richoz. Summary of early Triassic carbon isotope records. *Comptes Rendus Palevol*, 4(6-7):473–486, 2005.

[46] R. Petterson, A.R. Prave, B.P. Wernicke, and A.E. Fallick. The Neoproterozoic Noonday Formation, Death Valley region, California. *Geological Society of America Bulletin*, 123(7-8):1317–1336, 2011.

[47] F.A. Corsetti, S.M. Awramik, D.W. Pierce, and A.J. Kaufman. Using chemostratigraphy to correlate and calibrate unconformities in Neoproterozoic strata from the southern Great Basin of the United States. *International Geology Review*, 42(6):516 – 533, 2000.

[48] J.W. Hagadorn, C.M. Fedo, and B.M. Waggoner. Early Cambrian Ediacaran-type fossils from California. *Journal of Paleontology*, 74(4):731–740, 2000.

[49] J.W. Hagadorn and B. Waggoner. Ediacaran fossils from the southwestern Great Basin, United States. *Journal of Paleontology*, 74(2):349–359, 2000.

[50] S.B. Pruss, F.A. Corsetti, and W.W. Fischer. Seafloor-precipitated carbonate fans in the Neoproterozoic Rainstorm Member, Johnnie Formation, Death Valley Region, USA. *Sedimentary Geology*, 207(1-4):34–40, 2008.

[51] G.C. Bond, N. Christie-Blick, M.A. Kominz, and W.J. Devlin. An early Cambrian rift to post-rift transition in the Cordillera of western North America. *Nature*, 315(6022):742–746, 1985.

[52] M. Levy and N. Christie-Blick. Tectonic subsidence of the early paleozoic passive continental-margin in Eastern California and Southern Nevada. *Geological Society of America Bulletin*, 103(12):1590–1606, 1991.

[53] J.H. Stewart. Initial deposits in Cordilleran Geosyncline - evidence of a late Precambrian (less than 850 My) continental separation. *Geological Society of America Bulletin*, 83(5):1345, 1972.

[54] M.E. Clapham and F.A. Corsetti. Deep valley incision in the terminal Neoproterozoic (Ediacaran) Johnnie Formation, eastern California, USA: Tectonically or glacially driven? *Precambrian Research*, 141(3-4):154–164, 2005.

[55] C.M. Fedo and J.D. Cooper. Sedimentology and sequence stratigraphy of Neoproterozoic and Cambrian units across a craton-margin hinge zone, southeastern California, and implications for the early evolution of the Cordilleran margin. *Sedimentary Geology*, 141:501–522, 2001.

[56] J.H. Stewart. Extensional tectonics in the Death-Valley area, California - transport of the Panamint Range structural block 80-km northwestward. *Geology*, 11(3):153–157, 1983.

[57] T.C. Labotka, D. Bergfeld, and P.I. Nabelek. Two diamictites, two cap carbonates, two delta C-13 excursions, two rifts: The Neoproterozoic Kingston Peak Formation, Death Valley, California: Comment. *Geology*, 28(2):191–192, 2000.

[58] A.R. Prave. Two diamictites, two cap carbonates, two delta C-13 excursions, two rifts: The Neoproterozoic Kingston Peak Formation, Death Valley, California: Reply. *Geology*, 28(2):192–192, 2000.

[59] E.J. Trower and J.P. Grotzinger. Sedimentology, diagenesis, and stratigraphic occurrence of giant ooids in the Ediacaran Rainstorm Member, Johnnie Formation, Death Valley region, California. *Precambrian Research*, 180(1-2):113–124, 2010.

[60] P.A. Sandberg. Evaluation of ancient aragonite cements and their temporal distribution. *AAPG Bulletin-American Association of Petroleum Geologists*, 67(3):544–544, 1983.

[61] J.K. Snow and B.P. Wernicke. Cenozoic tectonism in the central basin and range: Magnitude, rate, and distribution of upper crustal strain. *American Journal of Science*, 300(9):659–719, 2000.

[62] B. Wernicke, G.J. Axen, and J.K. Snow. Basin and range extensional tectonics at the latitude of Las-Vegas, Nevada. *Geological Society of America Bulletin*, 100(11):1738–1757, 1988.

[63] F.A. Corsetti, D.L. Kidder, and P.J. Marenco. Trends in oolite dolomitization across the Neoproterozoic-Cambrian boundary: A case study from Death Valley, California. *Sedimentary Geology*, 191(3-4):135–150, 2006.